encit 2020

ABCM Associação Brasileira de Engenharia e Ciências Mecânicas

18th Brazilian Congress of Thermal Sciences and Engineering
November 16-20, 2020 (Online)

ENC-2020-0266
DIRECT NORMAL IRRADIANCE FORECASTING USING NUMERICAL WEATHER PREDICTION AND SEPARATION MODELS

João Humberto Serafim Martins [a, b]
Roberto Miguel Gutierrez Velásquez [a]
Fabricio Polifke da Silva [a]
[a] Facto Energy, 369 Haddock Lobo St., Rio de Janeiro, RJ, 20260-141, Brazil
joao.martins@factoenergy.com.br, roberto.velasquez@factoenergy.com; fabricio.polifke@factoenergy.com

Júlio César Passos [b]
[b] Laboratory of Energy Conversion Engineering and Energy Technology (LEPTEN), Department of Mechanical Engineering, Federal University of Santa Catarina (UFSC), Eng. Agronômico Andrei Cristian Ferreira St., Florianópolis, SC, 88040-900, Brazil
julio.passos@lepten.ufsc.br

Abstract. *The solar irradiation assessment, especially the Direct Normal Irradiance (DNI) component, represents a major step in the conception of Concentrated Solar Power (CSP) facilities, since they only take advantage of the DNI for power conversion. This process is vital to the accurate plant sizing and the power output estimate through its life cycle. Also, the DNI forecasting can reduce the power output uncertainty caused by solar irradiance intermittency, which leads to profitability gains and assists the facility operation and maintenance planning. In such a context, this study applies the Weather Research and Forecasting (WRF) model to assess the Global Horizontal Irradiance (GHI) within a 48-hour horizon. The site examined is Roque Gonzales, in southern Brazil, where a 250 kW-electrical rated power CSP plant is under development. GHI from the WRF model is dissociated in its beam and diffuse components with the application of the Boland-Ridley-Lauret (BRL) model, previously tuned to best fit the Brazilian weather. The forecasts performed better for clear skies, being the lowest overall errors obtained with the coarser spatial grid resolution. For clear skies, the Normalized Root Mean Square Error (nRMSE) ranged from 17% to 41% for GHI and 25% to 48% for DNI, while for cloudy conditions it ranged from 203% to 209% for GHI and from 218% to 237% for DNI, corroborating the challenges of cloudy weather forecasting.*

Keywords: *Direct Normal Irradiance, Numerical Weather Prediction, Weather Research and Forecasting, BRL model, Concentrated Solar Power*

1. INTRODUCTION

The solar radiation forecasting can benefit a Concentrated Solar Power (CSP) enterprise in multiple stages of its life cycle, from conception to operation. During the plant design, the correct estimation of the Direct Normal Irradiance (DNI) leads to a better dimensioning of the solar field and plant settings, while over its operation, short-term forecasts, known as nowcasting, assist in day-to-day decision making, in both cases helping to achieve more efficient outputs. Despite this, the mainstream weather forecasting techniques (i.e., Numerical Weather Prediction (NWP), satellite, sky cameras, and statistical) were initially developed to provide only Global Horizontal Irradiance (GHI) outputs (Blanco and Santigosa, 2017). NWP based methods are the benchmark for medium-term solar irradiance forecasting, from four hours up to six days ahead. In these methods, differential equations modeling the entire Earth's atmosphere are solved and provide estimates of its current and future conditions (Heller, 2017).

In recent years, some NWP models made possible predictions with DNI outputs (Heller, 2017). The study by Lopes et al. (2018) is an example of its application. The authors used the Integrated Forecasting System (IFS), an NWP model run by the European Centre for Medium-Range Weather Forecasts (ECMWF), to access straightforwardly the short-term DNI in southern Portugal. Similarly, Huertas-Tato et al. (2020) and Rodríguez-Benítez et al. (2020) used the WRF-solar configuration, which enables the Weather Research and Forecasting (WRF), to DNI forecasting. In the works of Lara-Fanego et al. (2012) and Nonnenmacher et al. (2016), the DNI is acquired through NWP models with post-processing, using additional outputs available in NWPs.

In contrast, this study proposes the assessment of the DNI employing NWP and separation models: first NWP models are applied to get the GHI within a 48-hour horizon. Then the Boland-Ridley-Lauret (BRL) model, developed by Ridley et al. (2010) to best fit south hemisphere locations, and adapted to the Brazilian climate by Lemos et al. (2017), is used to dissociate the beam and diffuse components from the GHI. The location evaluated is the Passo São

João hydroelectric complex, in Roque Gonzales, in the southernmost Brazilian state of Rio Grande do Sul, where a 250 kW_e Parabolic Trough Collector (PTC) CSP plant is under development. In this location, the average DNI is around 1,710 kWh/(m² year) or 4.7 kWh/(m² day) (LABREN, 2017), below the minimum 2,000 kWh/(m² year) often used as a sign of economic feasibility for CSP (IRENA, 2012). In later sections, the results are compared with locally acquired data, in order to calculate the prediction accuracy and compare it with the literature.

This study is associated with the Research and Development (R&D) project of the National Agency of Electric Energy (ANEEL) and CGT Eletrosul: "Development and Implementation of a 0.25 MW_e thermal solar plant". The project aims to analyze the performance and viability of a CSP facility in Southern Brazil and study the alternatives to make its insertion in the national energy matrix. The R&D scope includes a series of technical and academic studies, as the construction of the Roque Gonzales pilot plant.

2. IRRADIANCE FORECASTING

Although solar forecasting appears to be a general problem, it is highly site-dependent and its needs are under a strong influence from plant characteristics. Equation (1) presents the relation between DNI and the additional solar components, where k_d is the diffuse fraction, G_d is diffuse horizontal irradiance, G_b is the beam horizontal irradiance, G_n is the DNI, G is the GHI (given in W/m²) and θ_z is the zenith angle (Pereira et al., 2017).

$$k_d = \frac{G_d}{G} = \frac{G - G_b}{G} = \frac{G - G_n \cos\theta_z}{G} \tag{1}$$

Due to the dependence between power output and solar irradiance, their forecasting qualities are also widely correlated. This dependence affects plant operation activities in the short and very short-term, such as the generation schedule and dispatch strategies over the next minutes, hours, and days. Yet, through medium and long-term forecasts, it is possible to better plan preventive maintenance, accommodating them in periods with less prospect of generation, and optimize the site operation to increase power output or profitability (Law et al., 2016).

Even in different stages of a CSP project, the DNI accurate prediction can considerably improve its financial return. According to Law et al. (2016), for a 48-hour DNI forecast with a Root Mean Square Error (RMSE) between 325 and 400 W/m², for each 1 W/m² reduction, there is a financial return increase of 800 to 2,600 USD/year, for a plant with a solar multiple between 1.25 and 2, and a storage capacity between 0 and 20 hours. Likewise, for a Mean Absolute Error (MAE) between 250 and 300 W/m², each 1 W/m² decrease is equivalent to a revenue increase between 2,000 and 7,200 USD/year.

A typical forecasting system for a CSP plant employs several forecasting methods and information from local weather stations. Local measurements provide two contributions to a forecasting system: the continuous data supply for climatic condition databases, what enables, e.g., the application of statistical and Machine Learning (ML) algorithms, and the provision of real-time data, used in short and very short-term forecasts (Blanco and Santigosa, 2016).

2.1 Numerical Wheather Prediction

NWPs are models used and developed for weather forecasting. They describe the physical and dynamic processes in the atmosphere, being governed by known physical laws, such as energy and momentum conservation and hydrostatic continuity. As no analytical solutions are possible for the partial differential equations, they are solved numerically through the spatial domain discretization, using a three-dimensional grid (Heller, 2017).

These models can also simulate a past period, and its results compared with observed data, a process called reanalysis of NWPs (Blanco and Santigosa, 2017). The NWP models are the most suitable for forecasting solar irradiance on a time horizon between four hours and several days, as presented in Fig. (1). All the techniques mentioned have not been specifically developed for DNI forecasting. Yet, the DNI can be derived from GHI using global-to-beam models, also named as global-to-diffuse or separation models (Torres et al., 2010) or post-processing models (Law et al., 2014) using, e.g., statistical and ML techniques.

It is possible to classify the NWP models into two classes: global and mesoscale. A global model covers the whole Earth. The Global Forecast System (GFS) is the most popular global model. It requires an enormous amount of initialization data, provided by automatic recording performed by satellite observation systems and meteorological stations around the world. The model has a spatial resolution as small as half a degree (approximately 56 km at the Equator). Its outputs are available free and can input in a mesoscale model (NCEP, 2003). A mesoscale is a more detailed model and can feature extra information (e.g., topography, surface roughness, and albedo). The most extensive model is the Weather Research and Forecasting (WRF). The WRF is a code run by many universities and research organizations. It provides results for different altitudes, from the ground level to the stratosphere (UCAR, 2016; Blanco and Santigosa, 2017).

Besides being the only pure forecasting technique, NWPs are the best way to get reliable information about the future state of the meteorological variables needed for the simulation of a solar plant, e.g., temperature, humidity, and wind. (Blanco and Santigosa, 2017).

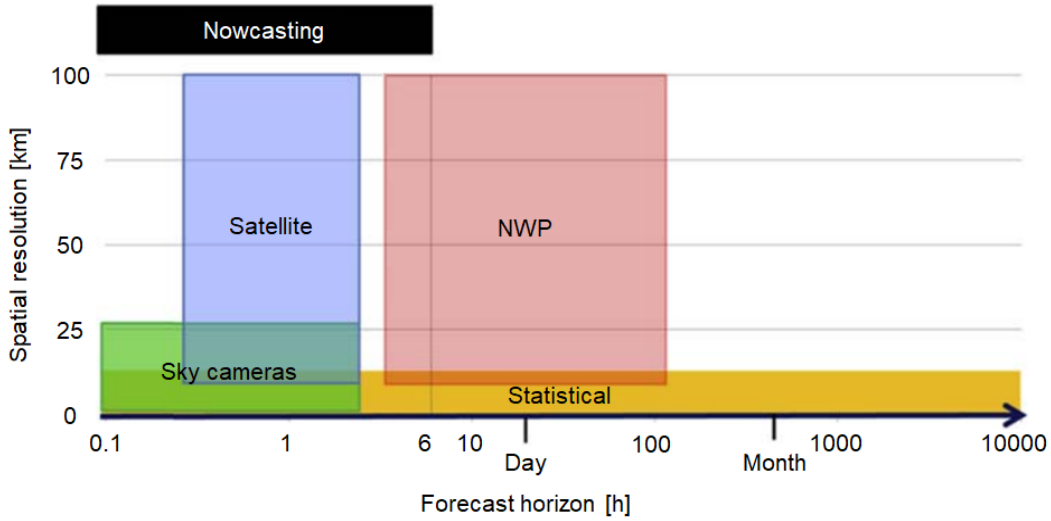

Figure 1. Main techniques for solar radiation forecasting with emphasis for their spatial and temporal resolutions. Adapted from Blanco and Santigosa (2017).

2.2 Boland-Ridley-Lauret model

According to Heller (2017), the Boland-Ridley-Lauret (BRL) model is one of the most frequently used separation models. Torres et al. (2010) compared 17 global-to-beam models and concluded the ablest to match the measured DNI were the DirInt, the Skartveit and Olseth, and the BRL, with RMSEs about, 46, 47, and 48 W/m², respectively.

The BRL model uses multiple parameters to estimate the fraction of Diffuse Horizontal Irradiance (DHI) present in the GHI, defined by Eq. (1). While most models are formulated only with data from the Northern Hemisphere, the BRL is based on measurements from several weather stations in Oceania and North America. Therefore, it presents better results for the southern hemisphere, compared to other commonly used models (Ridley et al., 2010). The model is governed by Eq. (2), where $\hat{k}_d$ is the predicted diffuse fraction, k_T is the hourly clearness index, AST is the apparent solar time, α is the solar altitude, K_T is the daily clearness index, and ψ is a persistence factor, defined in Ridley et al. (2010). The numeric values of β_i (β_0, β_1, …, β_5) are listed in Tab. (1).

$$\hat{k}_d = \frac{1}{1+e^{(\beta_0+\beta_1 k_T+\beta_2 AST+\beta_3 \alpha+\beta_4 K_T+\beta_5 \psi)}} \tag{2}$$

Lemos et al. (2017) developed the adjusted BRL model. Its coefficients were set to better represent the Brazilian weather, using measurements of global, diffuse and beam solar irradiance in nine meteorological stations, maintained by the National Institute for Space Research (INPE), within the scope of the National Organization System Project of Environmental Data (SONDA). However, it is important to emphasize this adjustment can be performed for any location, as long as appropriate data is used. Table (1) presents the original and the adjusted BRL model coefficients.

Table 1. Original BRL model coefficients for hourly data and its adjusted parameters for minute and hourly data in Brazil. Retrieved from Lemos et al. (2017).

Model	β_0	β_1	β_2	β_3	β_4	β_5	Author(s)
BRL – Hourly	-5.38	6.36	0.006	-0.00700	1.75	1.31	Ridley et al. (2010)
Adjusted BRL – Hourly	-4.41	7.87	-0.088	-0.00490	1.47	1.10	Lemos et al (2017)
Adjusted BRL – Minute	-6.26	5.97	0.024	-0.00533	2.84	2.41	Lemos et al (2017)

The predicted DNI ($\hat{G}_n$) is estimated through Eq. (3).

$$\hat{G}_n = \frac{(1-\hat{k}_d)G}{\sin\alpha} \tag{3}$$

3. CALCULATION POCEDURES

To assess the DNI, the methodology applied in this study underlies in the combination of the NWP and global-to-beam models. First, the GFS model was used to foresee the atmosphere's conditions, then its results were used as inputs in the WRF mesoscale NWP model to get the GHI forecasts. Finally, such results were inserted in the BRL model to be decomposed in their beam and diffuse portions.

The simulations were carried in a 48-hour horizon. In situ measurements were available, in a 10-minute resolution time series of GHI, DNI, and DHI, regarding the period between April 2014 and August 2017. Despite this, an hourly resolution was employed, as this is the NWP standard temporal resolution. Given the database characteristics, an uncertainty of about ±4.7% for the GHI can be assumed. All days simulated are contained in this period. The metrics considered to estimate the forecast accuracy were MAE, Mean Absolute Percentage Error (MAPE), Normalized Mean Absolute Percentage Error (nMAPE), RMSE and Normalized Root Mean Square Error (nRMSE).

MAE estimates the error average significance in a set of forecasting data, averaging the differences between the observations and the predictions from the entire sample. Similarly, the RMSE estimates the average error, based on the square root of the mean of the differences, squared between the predicted values and the actual observations. Therefore, the RMSE is more robust when dealing with large deviations, providing the ability to identify and eliminate outliers. In addition, the nRMSE is used in large datasets to assess general deviations from the sample (Ahmed et al., 2020). Both average indicators (MAE and RMSE) can result in non-negative values. MAPE and nMAPE are standard prediction techniques to measure the accuracy of forecasts, being the normalization recommended for larger datasets (Ahmed et al., 2020). Such metrics are calculated according to Eqs. (4) to (8), in which y_i and $\hat{y}_i$ are the measured and corresponding predicted values, respectively, and N is the number of test samples.

$$MAE = \frac{1}{N}\sum_{i=1}^{N}\left|y_i - \hat{y}_i\right| \tag{4}$$

$$MAPE = \frac{1}{N}\sum_{i=1}^{N}\frac{\left|y_i - \hat{y}_i\right|}{y_i} \tag{5}$$

$$nMAPE = \frac{1}{N}\sum_{i=1}^{N}\frac{\left|y_i - \hat{y}_i\right|}{\frac{1}{N}\sum_{i=1}^{N} y_i} \tag{6}$$

$$RMSE = \sqrt{MSE} = \sqrt{\frac{1}{N}\sum_{i=1}^{N}\left(y_i - \hat{y}_i\right)^2} \tag{7}$$

$$nRMSE = \frac{\sqrt{\frac{1}{N}\sum_{i=1}^{N}\left(y_i - \hat{y}_i\right)^2}}{\frac{1}{N}\sum_{i=1}^{N} y_i} \tag{8}$$

The WRF version used is the ARW 3.8, with the WRF Pre-Processing System (WPS) module (UCAR, 2016). The simulations applied the default settings, i.e., schematics 3 (WRF single-moment 3-class and 5-class) for cloud microphysics (Hong et al., 2004) and 1 (Kain-Fritsch) for convection parameterizations (Kain, 2004). Three spatial grids were addressed in the GFS model: d01 with 27 km, d02 with 9 km, and d03, with a 3 km resolution, containing the greater refinement. Figure (2) shows the generated grids for the GFS simulations in Roque Gonzales (RS).

From the time series, six 48-hour periods were randomly chosen, three of them with and three without significant cloud cover. The index used for this classification was the determination coefficient (R^2) between the extraterrestrial irradiance (G_0), calculated according to Duffie and Beckman (2013), and the observed GHI (G). The index is determined from the Eq. (9), where $\bar{y}$ is the average value. For high cloudiness, there is a lesser correlation between these variables. For determination coefficients higher or equal than 0.80, the days were labeled as clear sky, whereas days with lower coefficients were considered cloudy, as displayed in Fig. (3). The figure shows the solar irradiance components and the coefficient of determination between extraterrestrial irradiance and the measured GHI, calculated for the entire period. Such a procedure is proposed as an alternative to the use of the cloud cover index, which requires the image acquisition (Blanco and Santigosa, 2017), or the clearness index (Lara-Fanego et al., 2012).

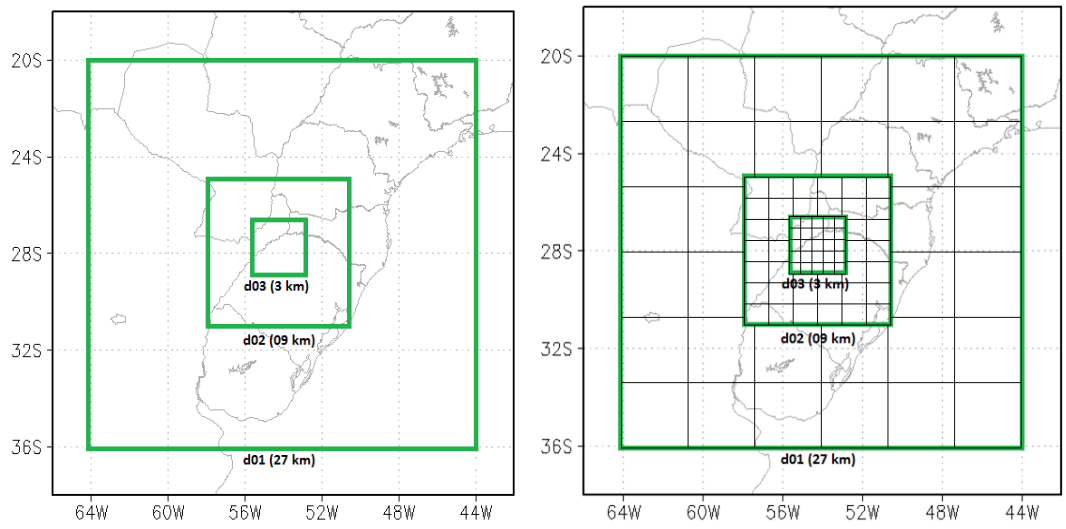

Figure 2. Depiction of the generated WRF grids.

$$R^2 = \frac{\sum_{i=1}^{N}\left(y_i - \hat{y}_i\right)^2}{\sum_{i=1}^{N}\left(y_i - \bar{y}_i\right)^2} \tag{9}$$

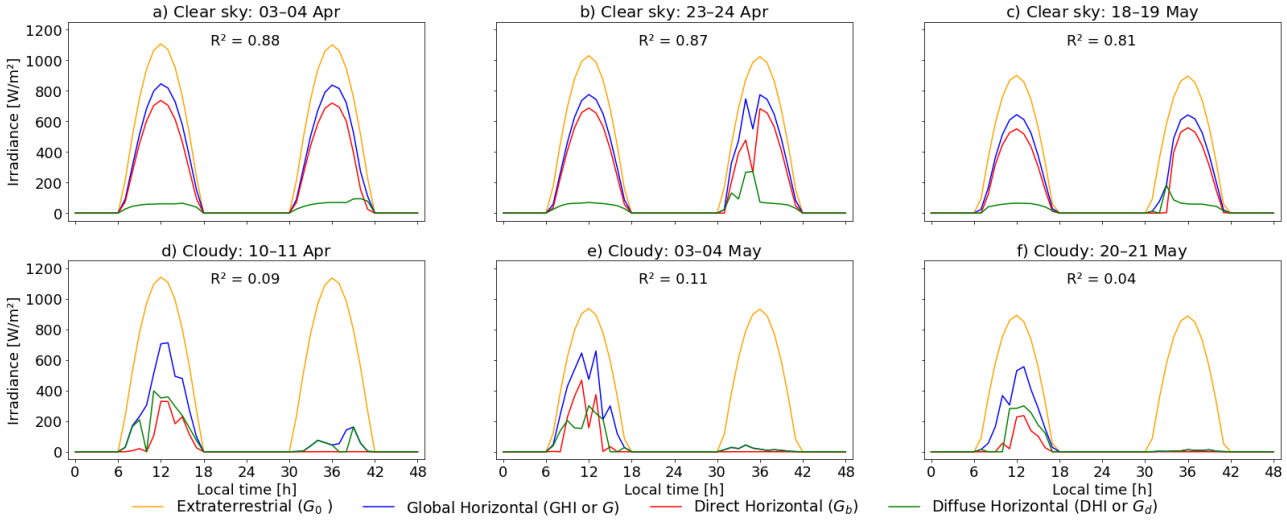

Figure 3. Components of solar irradiance. The coefficient of determination is relative to the GHI and the extraterrestrial irradiance in the entire period.

4. RESULTS

As described previously, the GFS model was used to foresee the atmosphere's state on an hourly basis. Then, these predictions were inserted into the WRF model, to more accurately foresee the GHI in Roque Gonzales. The predicted values of GHI ($\hat{G}$) are presented in Fig. (4). For clear skies, there is a slight difference among the GHI predicted by each grid, as seen by the overlapping lines. However, for cloudy skies it can be appreciated the NWP model is not able to precisely represent the atmospheric phenomena, being influenced by the grid size.

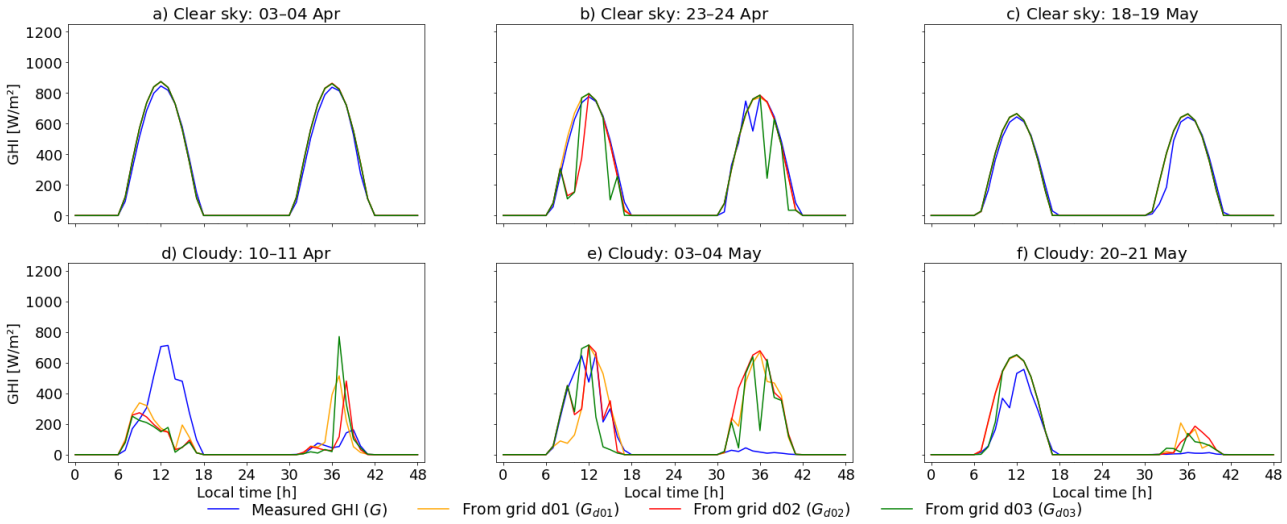

Figure 4. GHI forecast from the NWP model. Images *a)* to *c)* correspond to 48-hour horizon hourly predictions in clear sky days using three different spatial resolutions (grids d01, d02, and d03), whereas *d)* to *f)* correspond to cloudy days predictions.

Table (2) presents the GHI forecasting errors. The criteria used are the MAE, MAPE, nMAPE, RMSE and nRMSE, calculated according to Eqs. (4) to (8). The least refined grid, d01, results in the lowest MAEs and RMSEs for clear sky conditions (16 and 35 W/m², respectively) and all days, (46 and 118 W/m²), while the grid d03, the most refined, results in the lowest MAE and RMSE for the cloudy days (67 and 158 W/m²). These values corroborate the challenges of irradiance predictions using NWP described in the literature, mainly related to the atmosphere variability and cloud microphysics (Law et al., 2014; Blanco and Santigosa 2017).

Table 2. GHI forecast errors. MAE and RMSE in W/m², MAPE, nMAPE and nRMSE in percentage. The normalized errors are presented in brackets.

WRF grid	Clear sky			Cloudy			All		
	MAE	MAPE	RMSE	MAE	MAPE	RMSE	MAE	MAPE	RMSE
d01 (03 km)	16	22 (8)	35 (17)	75	254 (96)	163 (209)	46	295 (33)	118 (84)
d02 (09 km)	24	27 (12)	67 (33)	70	259 (90)	161 (207)	47	302 (34)	124 (88)
d03 (27 km)	30	30 (15)	83 (41)	67	216 (86)	158 (203)	48	256 (34)	126 (90)

Once the GHI predictions were obtained, calculations were performed to get the hourly DNI ($\hat{G}_n$), according to the Eqs. (2) and (3). The predicted DNI profiles can be seen in Fig. (5). Their forecasting errors shown in Tab. (3), were calculated similarly to those in Tab. (2). For clear skies, just as in the GHI forecast, there is a minor difference among the estimations by each grid, as the lines for the three grids are often overlapped.

For cloudy conditions, the prediction by each grid has greater disparity, being the DNI also influenced by the grid refinement, having more or less variability than in the GHI forecast, depending on the indicator analyzed. The spatial resolution influence on cloudy days can be attributed to the BRL model input, which comes from the WRF model, with a significant refinement sensitivity, as already mentioned.

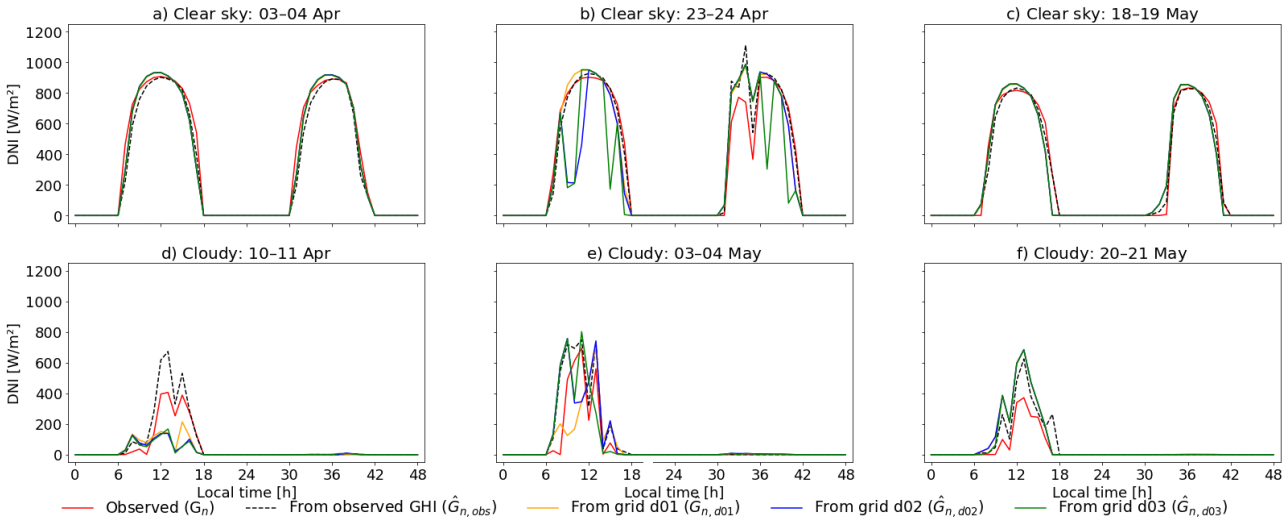

Figure 5. DNI forecast from the adjusted BRL model. Images *a)* to *c)* correspond to 48-hour horizon hourly predictions in clear sky days using three different spatial resolutions, whereas *d)* to *f)* correspond to cloudy days predictions. For comparison, the DNI obtained from the BRL model with observed GHI is also shown.

Regarding the errors, the coarser grid, d01, results in the lowest MAEs and RMSEs for clear and all sky conditions: for clear skies (34 and 74 W/m², respectively), and for all conditions (35 and 83 W/m²). For cloudy days the least and most refined grids present similar results MAE and RMSE results: 36 and 92 W/m² for d01, and 35 and 96 W/m² for d03, as observed in Tab. (3). The table also presents the errors from the BRL model application in the decomposition of observed GHI. For all sky conditions, the nRMSE is higher than the obtained by Lemos et al. (2017) using the adjusted BRL (16%), and the presented by Ridley et al. (2010) with the original BRL model (20%). This difference can be attributed both to the difference in the analyzed database sizes and quality, as well as to the low DNI in Roque Gonzales, which provides a relative increase in the normalized error metrics, such as nMAPE and nRMSE, as verified in Eqs. (6) and (8).

Table 3. DNI forecast errors. MAE and RMSE in W/m², MAPE, nMAPE and nRMSE in percentage. The normalized errors are presented in brackets.

GHI input	Clear sky			Cloudy			All		
	MAE	MAPE	RMSE	MAE	MAPE	RMSE	MAE	MAPE	RMSE
WRF grid d01	34	68 (11)	74 (25)	36	168 (85)	92 (218)	35	118 (20)	83 (49)
WRF grid d02	45	77 (15)	111 (37)	38	134 (89)	100 (237)	41	105 (24)	106 (62)
WRF grid d03	55	78 (19)	142 (48)	35	85 (82)	96 (228)	45	82 (27)	121 (71)
Observed [1]	26	56 (9)	63 (21)	25	213 (60)	74 (176)	25	134 (15)	69 (40)

[1] GHI data acquired in situ. Hence, the resultant DNI only present errors from the separation process

As noticed when comparing Tab. (2) and (3), it can be seen despite having the smallest forecast errors, the absolute indicators are more influenced by the cloudiness for GHI, while the normalized indicators tend to be more resilient to changes in the sky conditions, making the nMAPE and nRMSE vary further for DNI predictions, which is in accordance with Lara-Fanego et al. (2012).

In comparison to similar studies, it is worth mentioning the study of Lara-Fanego et al. (2012). Using the WRF model for GHI forecasting within a 24-hour horizon, it was verified nRMSEs about 10% and 50% for clear sky and cloudy days, respectively, whereas, for the DNI forecasting, it was verified around 20% and 100% clear sky and cloudy days. Using the WRF-solar, Huertas-Tato et al. (2020) got nRMSEs about 21% and 38% for GHI and DNI in a 6-hour horizon, and Rodríguez Benítz et al. (2020) reported nRMSE values to range from 25% to 70% for GHI and from 35% to 100% for DNI within a 6-hour horizon. Nonnenmacher et al. (2016), using NWP with post-processing, showed an nRMSE between 30% and 56% for day-ahead DNI predictions. Besides the mentioned works, Tab. (4) provide best performing forecasting models according to Law et al. (2014).

Table 4. Summary of best DNI forecast accuracy for appropriate forecasting horizons using NWP models. Accuracy measured by nRMSE, in percentage. Adapted from Law et al. (2014).

Author(s)	nRMSE for given horizon			Sky conditions
	24 h	48 h	72 h	
Wittmann et al. (2008); Lara-Fanego et al. (2012)	60–61%	42–62%	62–63%	All
Wittmann et al. (2008); Breitkreuz et al. (2009); Lara-Fanego et al. (2012); Ruiz-Arias et al. (2012)	6–31%	17–31%	-	Clear sky
Marquez and Coimbra (2011); Kraas et al. (2013)	31–33% (2)	56–77% (2)	-	All

(2) NWP with post-processing

5. CONCLUSIONS

In this study, simulations were performed to foresee the DNI in a southern Brazil location with a 48-hour horizon. The NWPs models were applied to forecast the GHI with an hourly resolution since it is more suitable for this timescale. WRF and GFS models were used for global and mesoscale simulations, respectively. Both have the advantage of being widely used and open-source. Subsequently, the adjusted BRL model was applied to get the DNI.

To better assess the prediction performance, this study considered three WRF grid dimensions: 27 km (d01), 9 km (d02), and 3 km (d03). Also, three cloud cover conditions were evaluated: clear sky, cloudy, and all sky conditions. The indicator used for this classification was the correlation coefficient between extraterrestrial irradiance and GHI for the first 24 hours. The DNI forecast was made for six periods, three of which classified as clear skies and three as cloudy. With a forecast horizon of 48 hours, 12 days were analyzed.

Both for GHI and DNI results show the best forecasts are obtained for the clear skies and the worst for cloudy conditions. Regarding spatial resolution, despite one can initially assume, the smallest forecasting errors were obtained, in general, by the coarsest grid, for clear skies and all days. The most refined grid, d03, presented better results in cloudy skies. For clear skies, the irradiance is governed by a well-behaved function. The grid refinement can introduce noise in the WRF model. Yet, in cloudy days, when highly non-linear phenomena occur, refining the spatial grid can boost the model predictive capacity.

When comparing the results with other studies also performing DNI prediction using NWPs, the proposed method did provide pleasing results for clear days, while it underperformed for cloudy conditions, since the nRMSEs for clear sky, cloudy, and all sky conditions are in the range between 25% and 48%, 218% and 237%, and 49% and 71%, respectively, while the reference, shown in Tab. (4), is between 17% and 31% for cloudy and 42% to 62% for all sky conditions. Such disparity can be assigned to challenges in cloudy weather forecasting, the difference in the database sizes and measurement uncertainties, and also to the low DNI in Roque Gonzales, about 1,710 kWh/(m² year), which may increase the normalized error metrics.

Therefore, this study contribution is related to the proposition of an alternative method for classifying days according to their cloudiness, using the correlation coefficient, and the combination of the GFS, WRF, and the adjusted-BRL models for DNI forecasting. Recognizing the study limitations, which covered the hourly prediction for just a few days, without considering seasonality effects, the forecast accuracy for cloudy days did not achieve the benchmark values for equivalent horizons. However, it is believed that it can still be improved. Since the models used are all open-source, there is great potential for further developments.

6. ACKNOWLEDGEMENTS

The authors acknowledge the support of ANEEL and CGT Eletrosul, through the R&D project entitled “Development and Implementation of a 0.25 MW_e thermal solar plant", which aims to meet the strategic R&D project call nº 19/2015. In addition, the authors acknowledge the support of the Coordination for the Improvement of Higher Education Personnel (CAPES), and CNPq (Process Number 406357/2013-7) which through the Federal University of Santa Catarina has supported LEPTEN research on CSP.

7. REFERENCES

Ahmed, R., Sreeram, V., Mishra, Y. and Arif, M.D, 2020. "A review and evaluation of the state-of-the-art in PV solar power forecasting: Techniques and optimization". *Renewable and Sustainable Energy Reviews*, Vol. 124, pp. 109792.

Blanco, M. and Santigosa, L.R., 2017. *Advances in Concentrating Solar Thermal Research and Technology*. Woodhead Publishing, [S.l.], 1st edition.

Breitkreuz, H., Schroedter-Homscheidt, M., Holzer-Popp, T. and Dech, S., 2009. "Short-Range Direct and Diffuse Irradiance Forecasts for Solar Energy Applications Based on Aerosol Chemical Transport and Numerical Weather Modeling". *Journal of Applied Meteorology and Climatology*, Vol. 48, No. 9, pp. 1766–1779.

Duffie, J.A and Beckman, W.A., 2013. *Solar engineering of thermal processes*. John Wiley & Sons, Hoboken, 4th edition.

Heller, P, 2017. *The Performance of Concentrated Solar Power (CSP) Systems*: Analysis, Measurement and Assessment. Woodhead Publishing, [S.l.], 1st edition.

Hong, S., Dudhia, J. and Chen, S., 2004. "A Revised Approach to Ice Microphysical Processes for the Bulk Parameterization of Clouds and Precipitation". *Monthly Weather Review*, Vol. 132, No. 1, pp. 103–120.

Huertas-Tato, J., Aler, Ricardo , Galván, I.M., Rodríguez-Benítez, F.J., Arbizu-Barrena, C. and Pozo-Vázquez D., 2020. "A short-term solar radiation forecasting system for the Iberian Peninsula. Part 2: Model blending approaches based on machine learning". *Solar Energy*, Vol. 195, pp. 685–696.

IRENA, 2012. *Renewable Energy Cost Analysis* - Concentrating Solar Power. International Renewable Energy Agency, Abu Dhabi, 1st edition.

Kain, J.S, 2004. "The Kain-Fritsch Convective Parameterization: An Update". *Journal of Applied Meteorology*, Vol. 43, No. 1, pp. 170–181.

Kraas, B., Schroedter-Homscheidt, M. and Madlener, R., 2013. "Economic merits of a state-of-the-art concentrating solar power forecasting system for participation in the Spanish electricity market". *Solar Energy*, Vol. 93, pp. 244–255.

LABREN, 2017. "Dados de irradiação para o estado do Rio Grande do Sul" Intituto Nacional de Pesquisas Espaciais. 16 Jun. 2020 <http://labren.ccst.inpe.br/atlas_2017_RS.html>.

Lara-Fanego, V., Ruiz-Arias, J.A., Pozo-Vázquez, D., Santos-Alamillos, F.J. and Tovar-Pescador, J., 2012. "Evaluation of the WRF model solar irradiance forecasts in Andalusia (southern Spain)". *Solar Energy*, Vol. 86, No. 8, pp. 2200–2217.

Law, E.W., Prasad, A.A., Kay, M. and Taylor, R.A., 2014. "Direct normal irradiance forecasting and its application to concentrated solar thermal output forecasting – A review". *Solar Energy*, Vol. 108, pp. 287–307.

Law, E.W., Kay, M., and Taylor, R.A., 2016. "Calculating the financial value of a concentrated solar thermal plant operated using direct normal irradiance forecasts". *Solar Energy*, Vol. 125, pp. 267–281.

Lemos, L.F.L., Starke, A.R., Boland, J., Cardemil, J.M., Machado, R.D. and Colle, S., 2017. "Assessment of solar radiation components in Brazil using the BRL model". *Renewable Energy*, Vol. 108, pp. 569–580.

Lopes, F.M., Silva, H.G., Salgado, R., Cavaco, A., Canhoto, P., Collares-Pereira, M., 2018. "Short-term forecasts of GHI and DNI for solar energy systems operation: assessment of the ecmwf integrated forecasting system in southern Portugal". *Solar Energy*, Vol. 170, pp. 14–30.

Marquez, R. and Coimbra, C.F.M., 2011. "Forecasting of global and direct solar irradiance using stochastic learning methods, ground experiments and the NWS database". *Solar Energy*, Vol. 85, No. 5, pp. 746–756.

NCEP, 2003. "The GFS Atmospheric Model" National Centers for Environmental Prediction. 15 Sep. 2020 <http://nws.noaa.gov/ost/climate/STIP/AGFS_DOC_1103.pdf>.

Nonnenmacher, L., Kaur, A. and Coimbra C.F.M., 2016. "Day-ahead resource forecasting for concentrated solar power integration". *Renewable Energy*, Vol. 86, pp. 866–876.

Pereira, E.B., Martins, F.R., Gonçalves, A.R., Costa, R.S., de Lima, F.J.L, Rüther, R., de Abreu, S.L., Tiepolo, G.M., Pereira, S.V. and de Souza, J.G., 2017. *Atlas Brasileiro de Energia Solar*. INPE, São José dos Campos, 2nd edition.

Ridley, B., Boland, J. and Lauret, P., 2010. "Modelling of diffuse solar fraction with multiple predictors". *Renewable Energy*, Vol. 35, No. 2, pp. 478–483.

Rodríguez-Benítez, F.J., Arbizu-Barrena, C., Huertas-Tato, J., Aler-Murb, R., Galván-León, I. and Pozo-Vázquez, D., 2020. "A short-term solar radiation forecasting system for the Iberian Peninsula. Part 1: Models description and performance assessment". *Solar Energy*, Vol. 195, pp. 396–412.

Ruiz-Arias, J.A., Gueymard, C.A., Dudhia, J. and Pozo-Vázquez, D., 2012. "Improvement of the weather research and forecasting (WRF) model for solar resource assessments and forecasts under clear skies". *In Proceedings of the World Renewable Energy Forum – WREF 2012*. Denver, United States of America.

Torres, J.L., de Blas, M., García, A. and and de Francisco, A., 2010. "Comparative study of various models in estimating hourly diffuse solar irradiance". *Renewable Energy*, Vol. 35, No. 6, pp. 1325–1332.

UCAR, 2016. "WRF Model Version 3.8" University Corporation for Atmospheric Research. 15 Sep. 2020 <http://www2.mmm.ucar.edu/wrf/users/wrfv3.8/wrf_model.html >.

Wittmann, M., Breitkreuz, H., Schroedter-Homscheidt, M. and Eck, M., 2008. "Case studies on the use of solar irradiance forecast for optimised operation strategies of solar thermal power plants". *IEEE Journal of Selected Topics in Applied Earth Observations and Remote Sensing,* Vol. 1, No. 1, pp. 18–27.

8. RESPONSIBILITY NOTICE

The authors are the only responsible for the printed material included in this paper.